Comparison of Hyper-reduction Methods combined with POD: Model Order Reduction of a Squirrel Cage Induction Machine in Nonlinear Case

T. Delagnes [2], T. Henneron [1], S. Clenet [1], M. Fratila [2] and J.P. Ducreux [2], *Senior member, IEEE*
[1]Univ. Lille, Arts et Metiers Institute of Technology, Centrale Lille, Junia, ULR 2697 - L2EP, F-59000 Lille, France
[2] EDF R&D, ERMES, 7 Boulevard Gaspard Monge, 91120 Palaiseau, France
E-mail: theo.delagnes@edf.fr

In an industrial context of electrical device design or expertise, it is common for engineer to use models based on the Finite Element (FE) method. In the case of nonlinear magneto-quasistatic problems, it can lead to prohibitive computational times. Then, Model Order Reduction (MOR) approaches based on the Proper Orthogonal Decomposition (POD) combined with a hyper-reduction method can be employed to reduce the computational time but often leads to numerical instabilities. In this article, we aim to compare two hyper-reduction methods that were developed to improve the stability of the nonlinear reduced model: the Gaussian Newton Augmented Tensors (GNAT) method and the Energy-Conserving mesh Sampling and Weighting (ECSW) method. The reduced models are evaluated in terms of accuracy on global and local quantities of interest and in terms of speedup, with application to a squirrel cage induction machine. Improvement of the ECSW method has been proposed such that it appears that this method is more competitive than the GNAT method and enables to obtain very good results both in terms of accuracy and time computation, which was reduced by a factor 40 compared to the FE model.

***Index Terms*—Nonlinear magneto-quasistatic problem, Finite Element Method, POD, GNAT, ECSW**

I. Introduction

To study the behaviour of electrical equipment, it is now common to use numerical simulations, in order to efficiently prepare or replace tests that are difficult or dangerous to carry out. In this context, the Finite Element (FE) method is used intensively for the study of low frequency electromagnetism problems, such as the simulation of transformers or electrical machines. It is based on the discretization of the Maxwell's equations leading to an differential algebraic equation system often of large size. The numerical solution is achieved step by step in order to obtain the time evolution of the fields and quantities of interest (fluxes, currents, losses, couple, etc.) necessary for equipment diagnosis. This tool is particularly interesting in an industrial context since it enables to build a High Fidelity (HF) model, which can be considered as a virtual prototype of the equipment, but is often very expensive in terms of computational time. To overcome this issue, it is necessary to reduce the computational time associated with the solving of the equation system. In the context of engineering sciences, model order reduction (MOR) methods have been developed for this purpose and are therefore well adapted to this type of problem.

The MOR methods are based on the definition of a reduced basis, defining a space of small dimension where an approximation of the FE solution is sought and which makes it possible to greatly reduce the size of the problem to solve (they will be referred as „projection" methods). These methods take advantage of the projection of the FE system in the reduced basis, and have often been developed for linear problems. Among the most known are the Proper Orthogonal Decomposition (POD) [1], the Proper Generalized Decomposition (PGD) [2], the Arnoldi method [3] and the Cauer Ladder Circuits [4]. However, in the case of nonlinear problems, the direct application of projection methods requires the reconstruction of the FE solution to evaluate the terms of the FE system (vector and/or matrix) at each iteration of the nonlinear loop, hindering the gain in terms of computational time provided by the reduction method.

To alleviate this issue, complementary methods have been developped recently to reduce the computational time associated with nonlinear problems. In the case of CLN, a method to account for the nonlinear behavior of ferromagnetic materials has been proposed and tested with success on an induction machine. It accounts for the nonlinearity of the ferromagnetic materials in the stator but not in the rotor. This method consists in introducing a nonlinear inductance in the equivalent circuit constructed by the CLN method. This modification is based on physical considerations. The nonlinear behavior is taken into account by considering a global quantity, i.e. the linkage flux, and not on the local values of the magnetic field [5]. Numerical methods enabling to reconstruct locally the magnetic field distribution, refered in the following as „hyper-reduction" methods have been also proposed. One approach to hyper-reduction consists in selecting a number of representative components (or points of space) on which nonlinear phenomena will be evaluated, and from which all non-linear vectors or matrices of the equation system will be reconstructed. The main methods are the oblique projection approaches based on Hyper-Reduction (HR) [6] such as Missing Point Estimation (MPE) [7], Discrete Empirical Interpolation Method (DEIM) [8], Gappy POD (GPOD) [9], Gaussian Newton Augmented Tensors (GNAT) [10] and Energy-Conserving mesh Sampling and Weighting (ECSW) [11]. Thanks to these approaches, it is possible to efficiently reduce the computational time associated with the simulation of nonlinear phenomena.

Nonetheless, the application and coupling of both projection and hyper-reduction methods is not trivial for most problems constructed from physical equations, as it can generate ill conditionned matrix system leading to convergence issues [12]. From our experience on a nonlinear non stationary problem, i.e. induction machine, the application of POD combined with

DEIM doesn't yield a stable reduced model, as the Newton-Raphson algorithm diverges when the nonlinear terms become non-negligible. Then, it has been shown in [13] that applying the GPOD method instead of DEIM can allow increasing the stability of the reduced model for some non stationary problems. However, in the case of the induction machine, we don't observe any significant improvement in the stability of the GPOD reduced model, which diverges as soon as the nonlinear terms become non-negligible.

In this context, HR methods were developped specificaly to be coupled with POD without degrading the stability of the nonlinear equation system. The GNAT method relies on the definition of a hierarchy of models, from the FE to the final MOR model, in order to ensure the consistency and optimality of the approximations, and was applied with success to computational fluid dynamics in [12]. The ECSW method consists in the selection of a small number of elements whose contributions are weighted to reconstruct the nonlinearities in the reduced system. It was adapted and compared to DEIM on an electromagnetic problem in [14], showing good performances in the case of problems where only parts of the domain are nonlinear. The efficiency of this method remains an open question in specific cases arising from industrial problems (i.e. induction machine simulation) : almost fully nonlinear domain, very large magnetic field variations, accounting for movement. In [15], the authors compared POD-DEIM, POD-GNAT and POD-ECSW structural dynamic models of a propeler blade and concluded that the two latest methods allow a better accuracy and stability of the reduced model. The behavior of the proposed approaches depends highly on the underlying physics

Hence, we propose to compare the GNAT and ECSW methods coupled with POD in the case of nonlinear magneto-quasistatic problem. We also propose an improvement of ECSW method in order to drastically reduce the computation time associated with the offline stage, which can be prohibitive. The targeted application is a squirrel cage induction machine where the nonlinearity play a key role in its electromechanical behavior.

In the first part, we present the construction of a FE system for a magneto-quasistatic problem, from the continuous domain to the discrete system of equations. In the second part, the projection method POD is detailed. In the third part, we introduce the two hyper-reduction methods GNAT and ECSW. In the fourth section, the methods are evaluated and compared on an industrial application case. The reduced model, constructed from the nominal operating point, is used for the simulation of faulty regimes of theinduction machine, to better assess the adequation of such reduced models to an industrial context. In the final part, concluding remarks are presented.

II. Magneto-quasistatic Problem

Let's consider a nonlinear magneto-quasistatic problem solved on $D \times [0,T]$, where D (Figure 1) is a domain of boundary $\Gamma = \Gamma_H \cup \Gamma_B$ (with $\Gamma_H \cap \Gamma_B = 0$) and T is the length of the time interval.

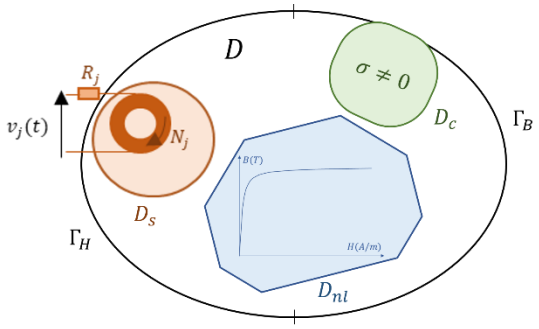

Figure 1. Nonlinear magneto-quasistatic problem

We define the source subdomain D_s composed of stranded windings, the conductive subdomain D_c and the nonlinear subdomain D_{nl} composed of ferromagnetic materials. The electrical conductivity $\sigma(\boldsymbol{x})$ is only non nul and constant on the conductive domain D_c elsewhere we have $\sigma(\boldsymbol{x})$. The problem is then defined by the following equations:

$$\boldsymbol{curl}\, \boldsymbol{H}(\boldsymbol{x},t) = \sigma(\boldsymbol{x})\boldsymbol{E}(\boldsymbol{x},t) + \sum_{j=1}^{N_{st}} \boldsymbol{N}_j(\boldsymbol{x}) i_j(t) \tag{1}$$

$$\boldsymbol{curl}\, \boldsymbol{E}(\boldsymbol{x},t) = -\frac{\partial \boldsymbol{B}(\boldsymbol{x},t)}{\partial t} \tag{2}$$

$$div\, \boldsymbol{B}(\boldsymbol{x},t) = 0 \tag{3}$$

$$\boldsymbol{H}(\boldsymbol{x},t) = \nu(\boldsymbol{B},\boldsymbol{x})\boldsymbol{B}(\boldsymbol{x},t) \tag{4}$$

with $\boldsymbol{B}$ the magnetic flux density, $\boldsymbol{H}$ the magnetic field, $\boldsymbol{E}$ the electric field, $\boldsymbol{N}_j$ and i_j the unit source vector and the current associated with the j^{th} winding, N_{st} the number of windings, $\sigma(\boldsymbol{x})$ the electric conductivity assumed to be constant and $\nu(\boldsymbol{B},\boldsymbol{x})$ the reluctivity which depends on the magnetic flux density in ferromagnetic material. The uniqueness of the solution is imposed through the boundary conditions, considering the outward unit normal vector $\boldsymbol{n}$:

$$\boldsymbol{H}(\boldsymbol{x},t) \times \boldsymbol{n} = 0 \; on \; \Gamma_H \;\text{ and }\; \boldsymbol{B}(\boldsymbol{x},t).\boldsymbol{n} = 0 \; on \; \Gamma_B \tag{5}$$

To impose the voltage v_j at the terminals of the winding j, the following circuit equation is added:

$$\frac{d\Phi_j(t)}{dt} + R_j i_j(t) = v_j(t) \tag{6}$$

with R_j the resistance of the winding j and Φ_j the linkage flux. Then, in the specific cases of rotating machines, the rotor movement shall be considered, and we define the rotation angle $\theta(t)$. Considering the 2D case, we then introduce the vector potential $\boldsymbol{A}$, which is defined from equations (2) and (3) as:

$$\boldsymbol{E}(\boldsymbol{x},t) = -\frac{\partial \boldsymbol{A}(\boldsymbol{x},t)}{\partial t} \;\text{ and }\; \boldsymbol{B}(\boldsymbol{x},t) = \boldsymbol{curl}\, \boldsymbol{A}(\boldsymbol{x},t) \tag{7}$$

The boundary conditions defined in (5) then transform to:

$$\begin{aligned} &\boldsymbol{curl}\, \boldsymbol{A}(\boldsymbol{x},t) \times \boldsymbol{n} = 0 \; on \; \Gamma_H \\ &\text{and } \boldsymbol{A}(\boldsymbol{x},t) \times \boldsymbol{n} = 0 \; on \; \Gamma_B \end{aligned} \tag{8}$$

Combining the potential defined as (7) with the problem defined by equations (1) to (4) and the circuit equation (5), we obtain the following matrix system to solve [22]:

$$\boldsymbol{curl}\,[\nu[\boldsymbol{curl}\,\boldsymbol{A}(\boldsymbol{x},t),x]\boldsymbol{A}(\boldsymbol{x},t)] = -\sigma(\boldsymbol{x})\frac{\partial \boldsymbol{A}(\boldsymbol{x},t)}{\partial t} + \sum_{j=1}^{N_{st}} \boldsymbol{N}_j(\boldsymbol{x}) i_j(t) \quad (9)$$

$$\frac{\partial}{\partial t}\int_{D_s} \boldsymbol{A}(\boldsymbol{x},t)\boldsymbol{N}_j(\boldsymbol{x})dD_s + R_j i_j(t) = v_j(t) \quad (10)$$

In the 2D case, the vector potential $A(\boldsymbol{x},t)$ can be chosen to have only one component normal to the 2D plane, the two components of the magnetic flux density are then given by $B_x(\boldsymbol{x},t) = \frac{\partial A(\boldsymbol{x},t)}{\partial y}$ and $B_y(\boldsymbol{x},t) = -\frac{\partial A(\boldsymbol{x},t)}{\partial x}$. To numerically solve this problem in 2D, we discretize $\boldsymbol{A}(\boldsymbol{x},t)$ and the vectors $\boldsymbol{N}_j(\boldsymbol{x})$ for $j = 1, \dots, N_{st}$ using fisrt order nodal functions and functions constant per element respectively. We then refer to the value of $\boldsymbol{A}$ at the ith node as $A_i(t)$, and introduce the set $\boldsymbol{\xi}$ and number N_ξ of elements and number of degrees of fredom (dof) associated with nodes N_A. Applying the weighted residue and Ritz-Galerkin methods to the problem defined by equations (9) and (10), we can construct the following differential algebraic equation system:

$$\left[\boldsymbol{M}\big(\boldsymbol{X}(t)\big) + \boldsymbol{M}^{ovl}\big(\theta(t)\big)\right]\boldsymbol{X}(t) + \boldsymbol{K}\frac{d\boldsymbol{X}(t)}{dt} = \boldsymbol{F}(t) \quad (11)$$

where $\boldsymbol{X}(t)$ is the vector of size $N = N_A + N_{st}$ gathering the unknowns $A_i(t)$ and $i_j(t)$. The $N \times N$ matrixes $\boldsymbol{M}$ and $\boldsymbol{K}$ respectively take into account the magnetic and electric behavior, whilst $\boldsymbol{M}^{ovl}$ allows considering the movement of the rotor, using the overlapping method in our case [16].To account for the movement of the stator and rotor, we use a Lagrangian approach. The matrix $\boldsymbol{M}^{ovl}$ enables to "connect" the meshes of the stator and the rotor accounting for the rotation angle of the rotor. The vector $\boldsymbol{F}$ of size N corresponds to the voltage source of the stranded inductors. We apply an Euler implicit time discretization scheme coupled with a Newton-Raphson approach to solve (11).

From the system (11) we can define the nonlinear vector $\boldsymbol{G}\big(\boldsymbol{X}(t)\big) = \boldsymbol{M}\big(\boldsymbol{X}(t)\big)\boldsymbol{X}(t) \in \mathbb{R}^N$, which is calculated as the sum of all elementary contributions. To explicitly describe the calculation of the nonlinear vector, let us a consider an element $e \in \boldsymbol{\xi}$ of the mesh connected to $n_A(e)$ nodes $(a_{p_1}, a_{p_2}, \dots, a_{p_{n_A(e)}})$, where p_j is the index of the jth edge connected to the element e. Then, the elementary contribution $\boldsymbol{g}_e\big(\boldsymbol{X}_e(t)\big) \in \mathbb{R}^{n_A(e)}$ is calculated from the curl-curl matrix $\boldsymbol{C}_e\big(\boldsymbol{X}_e(t)\big) \in \mathbb{R}^{n_A(e)\times n_A(e)}$ (discrete counterpart of the operator $\boldsymbol{curl}\,\nu\,\boldsymbol{curl}$ in (9)) ; and $\boldsymbol{X}_e(t) \in \mathbb{R}^{n_A(e)}$ the restriction of $\boldsymbol{X}(t)$ to the nodes $(a_{p_1}, a_{p_2}, \dots, a_{p_{n_A(e)}})$:

$$\boldsymbol{g}_e\big(\boldsymbol{X}_e(t)\big) = \boldsymbol{C}_e\big(\boldsymbol{X}_e(t)\big)\boldsymbol{X}_e(t) \quad (12)$$

To assemble the nonlinear vector, we then use the localisation matrix $\boldsymbol{L}_e \in \mathbb{R}^{N\times n_A(e)}$ constructed from the lines of the identity matrix of indices $(p_1, p_2, \dots, p_{n_A(e)})$:

$$G\big(\boldsymbol{X}(t)\big) = \sum_{e\in\xi} \boldsymbol{L}_e\, \boldsymbol{g}_e\big(\boldsymbol{X}_e(t)\big) \quad (13)$$

III. Projection of the system

To reduce the computational time associated with the solving of (11), we apply the POD method associated with the snapshot approach, using the "structure preserving" paradigm [17] which means that the unknowns related to the vector potential (stored in the N_A vector $\boldsymbol{X_A(t)}$) are considered separately from the unknowns related to the currents (stored in the currents vector $\boldsymbol{I}(t) = \big(i_1(t), i_2(t), \dots, i_{N_{st}}(t)\big)$). We solve (11) for N_s time steps and concatenate the vector $\left(\boldsymbol{X_A}^k\right)_{\boldsymbol{1<k<N_s}}$, where $\boldsymbol{X_A}^k$ is the solution at the k^{th} time step, to construct the snapshot matrix $\boldsymbol{S} \in \mathbb{R}^{N_A\times N_s}$. As the number of stranded inductors is usually low compared to the number of unknowns contains in the vector $\boldsymbol{X_A(t)}$, it is not necessary to construct a reduced basis for the currents vector $\boldsymbol{I}(t)$. Then, applying the Singular Value Decomposition, $\boldsymbol{S}$ can be written as:

$$\boldsymbol{S} = \boldsymbol{U\Sigma V}^t \quad (14)$$

With $\boldsymbol{U} \in \mathbb{R}^{N_A\times N_A}$ and $\boldsymbol{V} \in \mathbb{R}^{N_s\times N_s}$ matrices of orthogonal vectors, and $\boldsymbol{\Sigma} \in \mathbb{R}^{N_A\times N_s}$ a diagonal matrix containing the singular values ranked in descending magnitude. A reduced basis $\boldsymbol{\Psi} \in \mathbb{R}^{N\times m}$ can be constructed from $\boldsymbol{U}_{:n}$ the n first vectors of $\boldsymbol{U}$, and extended to account for the current vector $\boldsymbol{I}(t)$ with:

$$\boldsymbol{\Psi} = \begin{bmatrix} \boldsymbol{U}_{:n} & \boldsymbol{0} \\ \boldsymbol{0} & \boldsymbol{I}_d \end{bmatrix} \quad (15)$$

where $\boldsymbol{I}_d$ is the identity matrix of size $N_{st} \times N_{st}$. Then we define $\widetilde{\boldsymbol{X}}(t)$ an approximation of $\boldsymbol{X}(t)$ by the vector $\boldsymbol{X}_r(t) \in \mathbb{R}^m$ (with $m = n + N_{st} \ll N$) such that:

$$\boldsymbol{X}(t) \approx \widetilde{\boldsymbol{X}}(t) = \boldsymbol{\Psi}\boldsymbol{X}_r(t) \quad (16)$$

Then, injecting the approximation (16) in the FE system (11) and applying a Ritz-Galerkin projection, we can derive a reduced model:

$$\left[\boldsymbol{M_r}\left(\widetilde{\boldsymbol{X}}(t)\right) + \boldsymbol{M}_r^{ovl}\big(\theta(t)\big)\right]\boldsymbol{X}_r(t) + \boldsymbol{K}_r\frac{\partial \boldsymbol{X}_r(t)}{\partial t} = \boldsymbol{F}_r(t) \quad (17)$$

where $\boldsymbol{M_r}(\cdot) = \boldsymbol{\Psi}^t\boldsymbol{M}(\cdot)\boldsymbol{\Psi}$, $\boldsymbol{M}_r^{ovl}(\cdot) = \boldsymbol{\Psi}^t\boldsymbol{M}^{ovl}(\cdot)\boldsymbol{\Psi}$ and $\boldsymbol{K}_r = \boldsymbol{\Psi^t K \Psi}$ of size $m \times m$ are the reduced matrices, and $\boldsymbol{F}_r(\cdot) = \boldsymbol{\Psi}^t\boldsymbol{F}(\cdot) \in \mathbb{R}^m$ the reduced source vector. As presented in the case of the full FE model, we can define the reduced nonlinear vector $\boldsymbol{G_r}\left(\widetilde{\boldsymbol{X}}(t)\right) = \boldsymbol{M_r}\left(\widetilde{\boldsymbol{X}}(t)\right)\boldsymbol{X}_r(t) \in \mathbb{R}^m$ that is calculated from (13) as:

$$\boldsymbol{G}_r\left(\widetilde{\boldsymbol{X}}(t)\right) = \boldsymbol{\Psi}^t \sum_{e\in\xi} \boldsymbol{L}_e\, \boldsymbol{g}_e\left(\widetilde{\boldsymbol{X}}_e(t)\right) \quad (18)$$

The reduced system (17) has been drastically reduced with a number of unknows much lower than the FE system (11), allowing a faster resolution.

Nonetheless, the computational complexity of $\boldsymbol{G}_r\left(\widetilde{\boldsymbol{X}}(t)\right)$ is still significant, as it requires the following calculations at each time step, for each iteration of the Newton-Raphson algorithm to solve the nonlinear system (16):

1. Reconstruction of the FE solution approximation $\widetilde{\boldsymbol{X}}(t)$ using (16),

2. Loop through all elements $e = 1, \dots, N_\xi$ to calculate each individual contribution $\boldsymbol{g}_e\left(\widetilde{\boldsymbol{X}}_e(t)\right)$ and construct the nonlinear vector $\boldsymbol{G}\left(\widetilde{\boldsymbol{X}}(t)\right)$,
3. Projection in the reduced basis to deduce $\boldsymbol{G}_r\left(\widetilde{\boldsymbol{X}}(t)\right) = \boldsymbol{\Psi}^t \boldsymbol{G}\left(\widetilde{\boldsymbol{X}}(t)\right)$.

Each of these calculations is associated with a complexity that depends on either N_ξ or N, generating important computational time, that can completely counteract the acceleration from the reduction of the number of unknowns. To alleviate this issue, a hyper-reduction approach is investigated.

IV. Hyper-Reduction

We present two different methods used to reduce the computational burden of the nonlinear matrix: GNAT and ECSW.

A. GNAT

To accelerate the construction of $\boldsymbol{G}_r(\cdot)$, we aim to combine projection and interpolation, similarly to more commonly used methods such as DEIM or GPOD, to define an approximation of the reduced nonlinear vector. Using a mask $\boldsymbol{Z} \in \mathbb{R}^{N_z \times N}$ which is the concatenation of N_z lines of indexes $\{z_1, \dots, z_{N_z}\}$ of the identity matrix, we select N_z nodes of the mesh for which the nonlinear contributions of the set $\boldsymbol{\chi}$ of N_χ neighbor elements (see Figure 2) will be calculated:

$$\boldsymbol{G}_{|\boldsymbol{Z}}(\cdot) = \boldsymbol{Z}\boldsymbol{G}(\cdot) = \sum_{e \in \boldsymbol{\chi}} \boldsymbol{L}_e \, \boldsymbol{g}_e(\cdot) \tag{19}$$

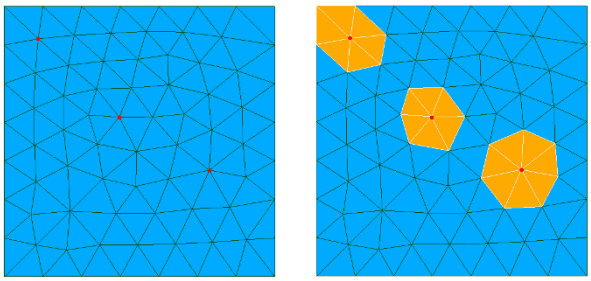

Figure 2. Example of a 2D mesh (a) with 3 selected nodes in red (b) and the associated set of neighbor elements $\boldsymbol{\chi}$ in orange

Then, an interpolation matrix $\boldsymbol{Q}$ is used to construct the approximation of the reduced nonlinear vector with:

$$\widetilde{\boldsymbol{G}}_r^{GNAT}(\cdot) = \boldsymbol{Q}\boldsymbol{G}_{|\boldsymbol{Z}}(\cdot) \tag{20}$$

To deduce the mask $\boldsymbol{Z}$ and define the interpolation matrix $\boldsymbol{Q}$, a reduced basis is constructed specifically for the nonlinear vectors, using the snapshot approach presented in III. Classically when applying the DEIM or GPOD [13], the FE system (11) is solved for N_c time steps and the nonlinear vectors $\boldsymbol{G}(\boldsymbol{X}^k)$ are concatenated in a snapshot matrix $\boldsymbol{C} \in \mathbb{R}^{N \times N_c}$. We apply a SVD on $\boldsymbol{C}$ and choose a truncation rank m_b to define the basis of nonlinear vectors $\boldsymbol{\Pi} \in \mathbb{R}^{N \times m_b}$. Then, the mask $\boldsymbol{Z}$ can be deduced by maximizing the volume of the submatrix $\boldsymbol{Z}\boldsymbol{\Pi}$, using either a LU or a QR decomposition on $\boldsymbol{\Pi}$ and extracting the indexes of the permutation matrix [18]. Finally, the interpolation matrix $\boldsymbol{Q} \in \mathbb{R}^{m \times N_z}$ is defined by:

$$\boldsymbol{Q} = \boldsymbol{\Psi}^t \boldsymbol{\Pi} [\boldsymbol{Z}\boldsymbol{\Pi}]^+ \tag{21}$$

with $[\boldsymbol{P}]^+$ being the pseudo-inverse of the matrix $\boldsymbol{P}$. The approximation (20) only requires evaluating the contributions of a reduced number of elements $N_\chi \ll N_\xi$, and the calculation of the product with the interpolation matrix $\boldsymbol{Q}$, offering an important reduction of the computational time.

The GNAT approach is quite different from the previous approaches which can lead to numerical instabilities [12]. The GNAT approach consists in a thorough methodology for the construction of $\boldsymbol{\Psi}$, $\boldsymbol{Z}$ and $\boldsymbol{\Pi}$, ensuring the consistency and optimality of the approximations (16) and (20). It introduces a hierarchy of models where, at each step, an approximation is introduced to define the next one, as depicted in Figure 3.

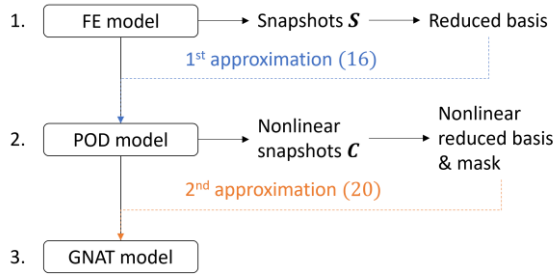

Figure 3. Hierarchy of models and approximations

In step 1., we solve the FE system (11) to generate N_s snapshots defined as $\Delta \boldsymbol{X_A}^k = \boldsymbol{X_A}^k - \boldsymbol{X_A}^{k-1}$, so-called „increments" in the following where $\boldsymbol{X_A}^k$ corresponds to the solution at the time step k. The increments are stored in a snapshot matrix $\boldsymbol{S}$ on which we apply the SVD as described in III to construct the reduced basis $\boldsymbol{\Psi}$ of size m using (15), ensuring the consistency of the approximation (16), meaning that implemented without snapshot compression, it introduces no additional error in the solution at the training points.

Then in step 2., we solve the reduced system (17) to generate N_c nonlinear vectors $\boldsymbol{G}(\widetilde{\boldsymbol{X}}^k)$ merged to a snapshot matrix $\boldsymbol{C}$. As they were generated by the POD model, these nonlinear vectors take into account the approximation (16). Then, the basis of nonlinear vectors $\boldsymbol{\Pi}$ of size m_b is computed applying the SVD on $\boldsymbol{C}$, and the mask $\boldsymbol{Z}$ of size N_z is deduced by means of a QR decomposition on $\boldsymbol{\Pi}$. Finally, we can construct the interpolation matrix with (21).

In step 3., we can use the GNAT model to solve (17), taking advantage of the gain in computational time offered by the approximation (20).

B. ECSW

Another approach to speed up the computation of the reduced nonlinear vector $\boldsymbol{G}_r(\cdot)$ consists in approximating it from the weighted contributions of a low number of selected elements, applying the ECSW method. Let us introduce $\boldsymbol{\epsilon} \subset \boldsymbol{\xi}$ a set of N_ϵ elements and $\boldsymbol{\zeta} = (\zeta_1, \dots, \zeta_{N_\epsilon})$ the associated set of positive weights. Then, from the definition of the reduced nonlinear vector (*18*) based on the sum of the contributions of all

elements, we can define an approximation by only considering the weighted contributions of the elements of $\boldsymbol{\epsilon}$:

$$\widetilde{\boldsymbol{G}}_r^{ECSW}(\cdot) = \boldsymbol{\Psi}^t \sum_{e \in \boldsymbol{\epsilon}} \boldsymbol{L}_e \zeta_e \boldsymbol{g}_e(\cdot) \tag{22}$$

Firstly, as described in III, we solve (*11*) to generate N_s snapshots in the matrix $\boldsymbol{S}$ and deduce a reduced basis $\boldsymbol{\Psi}$ of size m by means of truncated SVD. It should be mentioned that incremental snapshots can also be used in the ECSW method as in the GNAT method. Numerical experiments show that we obtain very similar results than the ones obtained using snapshots of the solution of the FE problem. Then, we choose $N_p \leq N_s$ vectors in $\boldsymbol{S}$ that will allow to calculate different values of the nonlinear contributions $\boldsymbol{g}_e(\cdot)$. For each selected vector $\boldsymbol{X_A}^k$ we calculate the reconstruction $\overline{\boldsymbol{X_A}}^k$ in the basis $\boldsymbol{\Psi}$ (to account for the approximation) with:

$$\overline{\boldsymbol{X_A}}^k = \boldsymbol{\Psi}^t \boldsymbol{\Psi} \boldsymbol{X_A}^k \tag{23}$$

Then, we define $\overline{\boldsymbol{X_e}}^k \in \mathbb{R}^{n_A(e)}$ the restriction of $\overline{\boldsymbol{X_A}}^k$ to the nodes $(a_{p_1}, a_{p_2}, \dots, a_{p_{n_A(e)}})$ (see (12)). We define the projected elementary contribution $\boldsymbol{D}_{k,e}$ which is a vector of size m, concatenated in the matrix $\boldsymbol{D} \in \mathbb{R}^{(m \cdot N_p) \times N_\xi}$ such that:

$$\boldsymbol{D}_{k,e} = \begin{pmatrix} d_{k,e}^1 \\ \vdots \\ d_{k,e}^m \end{pmatrix} = \boldsymbol{\Psi}^t \boldsymbol{L}_e \boldsymbol{g}_e \left(\overline{\boldsymbol{X_e}}^k \right)$$
$$\boldsymbol{D} = \begin{bmatrix} \boldsymbol{D}_{1,1} & \cdots & \boldsymbol{D}_{1,N_\xi} \\ \vdots & \vdots & \vdots \\ \boldsymbol{D}_{j,1} & \cdots & \boldsymbol{D}_{j,N_\xi} \\ \vdots & \vdots & \vdots \\ \boldsymbol{D}_{N_p,1} & \cdots & \boldsymbol{D}_{N_p,N_\xi} \end{bmatrix} \tag{24}$$

and we can calculate the assembled contributions vector $\boldsymbol{b} \in \mathbb{R}^{(m \cdot N_p)}$:

$$\boldsymbol{b}_k = \begin{pmatrix} b_k^1 \\ \vdots \\ b_k^m \end{pmatrix} = \sum_{e \in \boldsymbol{\xi}} \boldsymbol{D}_{k,e}$$
$$\boldsymbol{b} = \begin{bmatrix} \boldsymbol{b}_1 \\ \vdots \\ \boldsymbol{b}_j \\ \vdots \\ \boldsymbol{b}_{N_p} \end{bmatrix} \tag{25}$$

We seek the weights $\boldsymbol{\zeta}$ that minimize the difference between the assembled contributions calculated from a small number of selected elements $\boldsymbol{\epsilon}$, and by all elements. Translating this into equation, the weights $\boldsymbol{\zeta}$ can then be obtained from $\boldsymbol{D}$ and $\boldsymbol{b}$ by solving the following minimization problem:

$$\boldsymbol{\zeta} = \arg\min_{\boldsymbol{\kappa} \in \boldsymbol{\phi}} \|\boldsymbol{\kappa}\|_0 \tag{26}$$
$$\boldsymbol{\phi} = \left\{ \boldsymbol{\kappa} \in \mathbb{R}^{N_\xi} : \|\boldsymbol{D}\boldsymbol{\kappa} - \boldsymbol{b}\|_2 < \|\tau \boldsymbol{b}\|_2 \, ; \boldsymbol{\kappa} > \boldsymbol{0} \right\} \tag{27}$$

In (27), τ is a tolerance parameter chosen by the user. An effective way to solve this minimization problem is by using the sparse Non-Negative Least Square (s-NNLS) algorithm [19], and the selected elements corresponds to those having a non-null weight.

Then, once we have calculated the reduced basis $\boldsymbol{\Psi}$ and the weights $\boldsymbol{\zeta}$, we can inject the ECSW approximation (22) in the reduced model in place of (18) to define the POD-ECSW model. As we only evaluate $N_{\boldsymbol{\epsilon}} \ll N_\xi$ contributions to construct the approximation of the reduced nonlinear vector, using the POD-ECSW model to solve (*17*) allows a significant gain in computational time.

However, looking at the important size of the elementary projected contributions matrix $\boldsymbol{D}$ in its definition (*24*), we can expect memory issues when trying to allocate it. Therefore, we will need to reduce its size, by lowering the value of the parameter N_p to a minimum. In this purpose, we propose to apply the k-means algorithm [20] to find a reduced number of representative vectors from the N_p vector chosen in $\boldsymbol{S}$. It merely consists in computing distances (in terms of the Frobenius norm) between vectors to gather close ones in small sets and represent each set by its center. The sets and centers are determined through an iterative process. The choice of this algorithm is motivated by its low computational time and ability to capture information.

V. APPLICATION

To compare the two hyper-reduction approaches, a 2D magneto-quasistatic example of a 500kW squirrel cage induction machine around its nominal operating point is studied. The spatial mesh constituted of 111833 elements associated to 72233 unknowns is presented on Figure 4 (left), where D_s corresponds to the stator inductors (the color indicating different phases), D_c to the bars (copper). Then, D_{nl} corresponds to the stator and rotor, whose nonlinear magnetic behavior are considered via the curve presented on Figure 4 (right). The Euler scheme and Newton-Raphson method are used to solve (11) with 180 time-steps per electrical period.

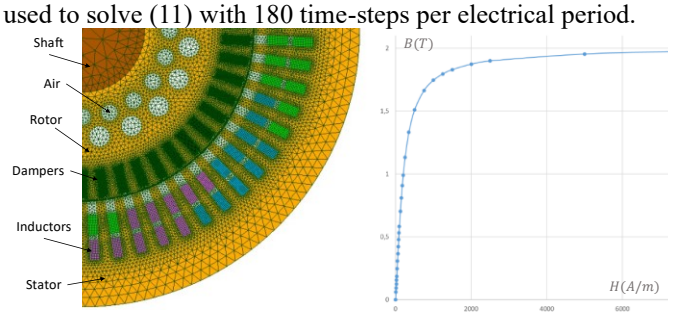

Figure 4. (left): quarter of the mesh with the three-phase winding (D_s) in green, blue and pink, rotor bars (D_c) in brown, ferromagnetic material (D_c) in orange; (right) nonlinear curve of rotor and stator).

In the following, we present results of the FE model and the construction of the reduced model for both GNAT and POD-ECSW. Then, we compare the results obtained by the reduced models to those of the FE model, which will be considered as the reference, for both healthy and faulty modes. All calculations run on a laptop with a i7-11850H @ 2.50GHz × 16 CPU, and all implementations are in FORTRAN90 based on the electromagnetic research FE code *code_Carmel*.

A. Results of a FE simulation

We perform a FE simulation of the induction machine, imposing nominal 50Hz voltage at the terminals of the windings and nominal rotation speed. Then, we focus on the time evolution of global quantities of interest: the currents in the windings (Figure 5), the electromagnetic torque (Figure 6), and

the eddy current losses (Figure 7). All these quantities are computed from the FE solution vectors and give valuable insights on the behavior of the machine.

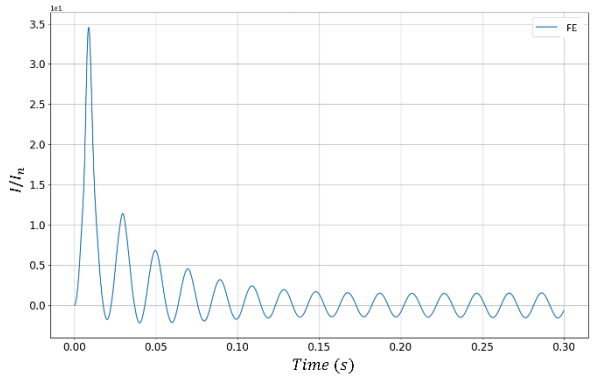

Figure 5. Current in the windings of phase 1 from FE model

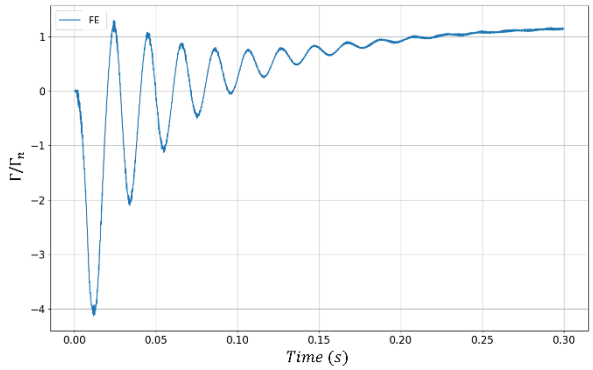

Figure 6. Electromagnetic torque from FE model

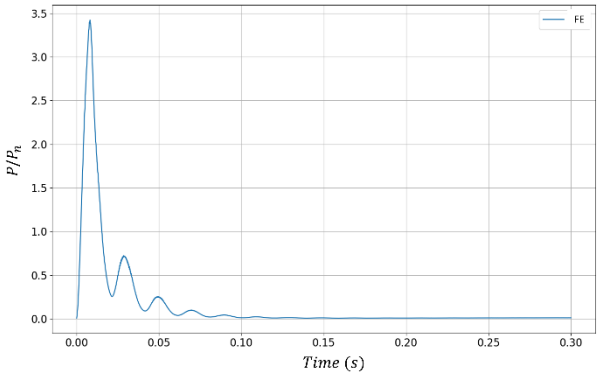

Figure 7. Eddy current losses from FE model

On these quantities, we can see a strong transient where the machine is highly saturated in the first 0.1s of simulation, slowly converging to the steady-state at 0.2s.

B. Construction of the GNAT model

To construct the reduced model using GNAT, we follow the steps presented on Figure 3 and described in IV.A. In step 1, we construct 2 snapshots matrices containing increment solutions of the FE simulation presented in V.A, collected during the transient state (6 electrical periods generating 1080 vectors in $\boldsymbol{S_{\Delta 1}}$) and the steady state (2 electrical periods generating 360 vectors in $\boldsymbol{S_{\Delta 2}}$). We deduce the bases $\boldsymbol{\Psi_{\Delta 1}}$ of size 25 and $\boldsymbol{\Psi_{\Delta 2}}$ of size 50 from these snapshots using SVD, choosing the sizes based on the analysis of the singular values (see Figure 8), and concatenate them to obtain the final reduced basis $\boldsymbol{\Psi_{\Delta}}$ of size $m = 75$. This choice is motivated by the observation that snapshots at the steady state regime are often considered of low energy by the SVD compared to the snapshots at the transient state. By separating the bases, and by setting a bigger size for the steady-state regime basis, the information of this regime will not be ignored. Indeed, we know from previous works [21] that it is the case, when the basis is deduced from a single snapshot matrix concatenating solutions from both states.

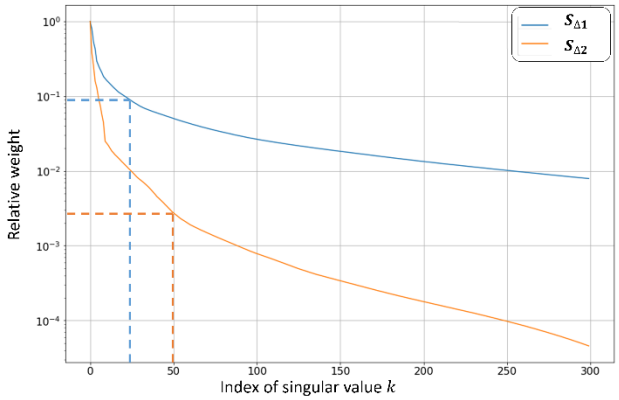

Figure 8. Relative weights of the singular values of $\boldsymbol{S_{\Delta 1}}$ and $\boldsymbol{S_{\Delta 2}}$

Then, in step 2 of the GNAT methodology, we perform a new simulation of the machine at its nominal operating point with the POD model constructed using $\boldsymbol{\Psi_{\Delta}}$**.** We generate nonlinear snapshots in the transient state (720 vectors corresponding to 4 electrical periods) saved in the matrix $\boldsymbol{C}$. Then, the nonlinear basis $\boldsymbol{\Pi}$ and mask $\boldsymbol{Z}$ are deduced using respectively SVD and QR decomposition, setting $m_b = 360$ and $N_z = 800$ (corresponding to 4708 neighbor elements). In total, the offline time of the approach (without the FE simulation presented in V.A) is 3 hours and 12 minutes.

C. Construction of the POD-ECSW model

To construct the POD-ECSW model, we collect solutions from the FE simulation presented in V.A, of the transient state in $\boldsymbol{S_1}$ (1080 vectors) and of the steady state in $\boldsymbol{S_2}$ (360 vectors). The only difference with the GNAT model construction is the use of solutions and not increments. Using SVD, we deduce the bases $\boldsymbol{\Psi_1}$ of size 25 and $\boldsymbol{\Psi_2}$ of size 50 and construct the final reduced basis $\boldsymbol{\Psi}$ of size $m = 75$ by concatenation (Figure 9).

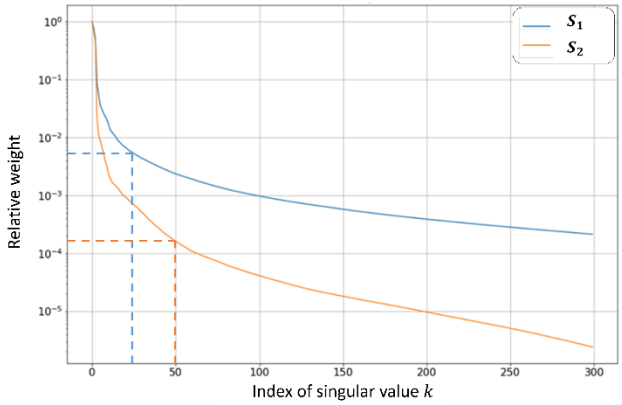

Figure 9. Relative weights of the singular values of $\boldsymbol{S_1}$ *and* $\boldsymbol{S_2}$

Then, we need to choose snapshots that will be used to construct the matrix $\boldsymbol{D}$ (*24*) and the vector $\boldsymbol{b}$ (*25*), to eventually deduce the selected elements and their associated weight. To reduce the offline time of the method, and as we know from experience that the information on nonlinear contributions is contained in the first electrical periods, we will only use the first 720 solutions from the first 4 electrical periods of the FE simulation presented in V.A in (*23*). However, looking at the definition of $\boldsymbol{D}$ and as discussed in IV.B, we must allocate memory for a 54000×111833 full matrix, which is prohibitive. To tackle this issue, and to further reduce the offline computational time of the method, we propose to lower the number of vectors used to construct $\boldsymbol{D}$ and $\boldsymbol{b}$ from 720 to 100. To do so, we apply the k-means algorithm [20] to find 100 representative vectors that will be used to construct $\boldsymbol{D}$ and $\boldsymbol{b}$, and then deduce the selected elements and weights with the s-NNLS algorithm. The parameter τ is fixed to 10^{-2} giving us $N_\epsilon = 333$ elements (corresponding to 862 node values), with an offline time of the method of 1 hour and 44 minutes (without the FE simulation presented in V.A). We can see that the time computation of the offline stage is lower than with the GNAT method, which takes 3 hours 12 minutes.

D. Comparison

1. Selected elements

As a first point of comparison, we present the selected elements (set $\boldsymbol{\chi}$ in the GNAT case, $\boldsymbol{\epsilon}$ in the ECSW case) in a small area of the mesh on Figure 10. We see that in both cases they are concentrated around the corner of the stator slots, as well as near the air gap of the machine, which are regions with an important variation of magnetic flux induction as well as a significant saturation.

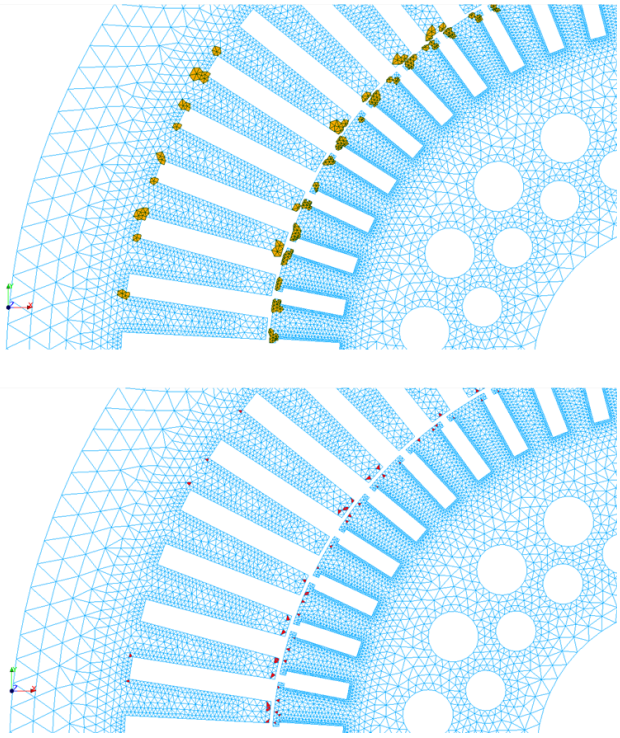

Figure 10. Top: set $\boldsymbol{\chi}$ *of elements connected to the selected nodes in the GNAT case (yellow), bottom: set* $\boldsymbol{\epsilon}$ *of elements selected in the ECSW case (red)*

2. Simulation at nominal regime

To compare the quality of the two reduced models, we perform the simulation imposing nominal 50Hz voltage at the terminals of the windings and nominal rotation speed with the GNAT model described in V.B and the POD-ECSW model described in V.C. Then, we compute quantities of interest in transient and steady state for both reduced models and compare to the reference of the FE model presented in V.A. We are interested in the electromagnetic torque Γ relatively to its nominal value and the eddy current losses P relatively to the nominal power of the machine, as well as the distribution of magnetic flux density $\boldsymbol{B}$. The time evolutions of the global quantities are presented on Figure 11 concerning the torque and Figure 12 for the eddy current losses. The magnetic flux density distribution in steady state regime of the FE model and the associated absolute error of the GNAT and ECSW models are shown on Figure 13.

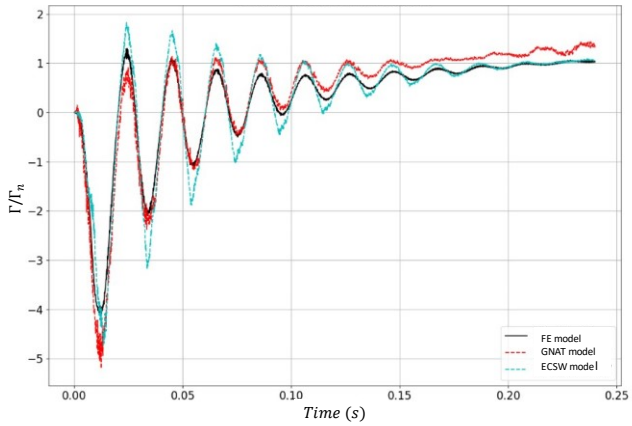

Figure 11. Electromagnetic torque from FE model (black), GNAT (red dashes) and ECSW (cyan dashes) in nominal regime

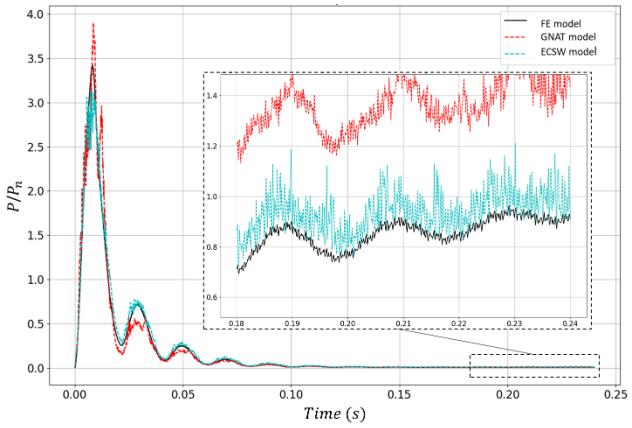

Figure 12. Eddy current losses from FE model (black), GNAT (red dashes) and ECSW (cyan dashes) in nominal regime

We can observe, looking at the electromagnetic torque and eddy current losses, a similar deviation on peak values for both GNAT and ECSW models in transient regime. In steady state however, the ECSW model yields a much smaller error ($< 5\%$ for torque, $\approx 10\%$ for losses) than the GNAT model ($\approx 25\%$ for torque, $\approx 60\%$ for losses). This is confirmed by the magnetic flux density distribution error, which is very small ($< 5\%$) and concentrated for the ECSW model but spreads across the entire domain in greater magnitude ($\approx 20\%$) for the GNAT model.

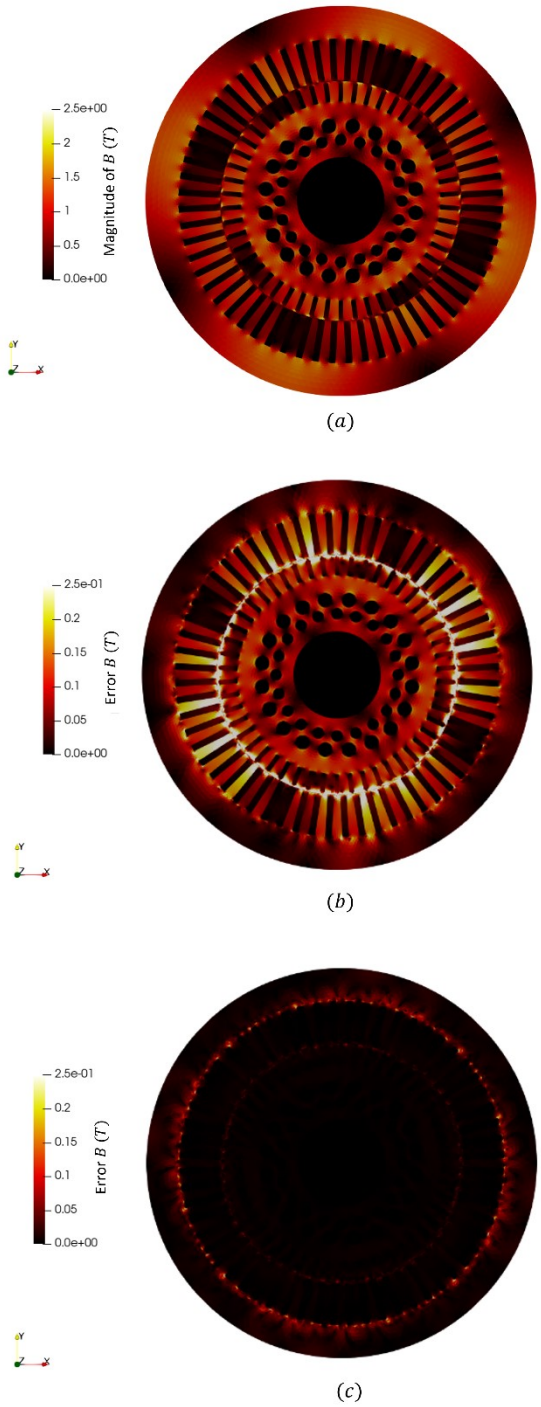

Figure 13. Magnetic flux density distribution in steady state in nominal regime (a: FE distribution, b: GNAT absolute error, c: ECSW absolute error)

3. Simulations in faulty regimes

To go further on comparison, we propose to evaluate the reduced models in the context of a typical industrial study, usually performed by engineers and requiring multiple FE simulations. It consists in simulating the induction machine in faulty operating modes close to the nominal, to evaluate the impact on global quantities such as eddy current losses. Indeed, with the help of a thermal model, this quantity enables to

calculate the overheating to evaluate the impact on the lifetime of the induction machine. Here we will focus on the influence of a drop of the supply voltage and therefore fix a range of voltages corresponding to the electrical machine specifications. To do so, we impose carefully chosen values of voltage magnitude U for the windings and rotor rotation speed ω (with U_n and ω_n the associated nominal values):

- at $U = 0.9U_n$ and $\omega = 0.998\omega_n$
- at $U = 0.8U_n$ and $\omega = 0.996\omega_n$

Then, we simulate these faulty regimes with the FE model to set a reference, and with the two reduced models constructed from the nominal operating point simulation : the GNAT model described in V.B and the POD-ECSW model described in V.C. The values of electromagnetic torque and eddy current losses are presented on Figure 14 and Figure 15 concerning the first faulty regime and on Figure 16 and Figure 17 concerning the second one.

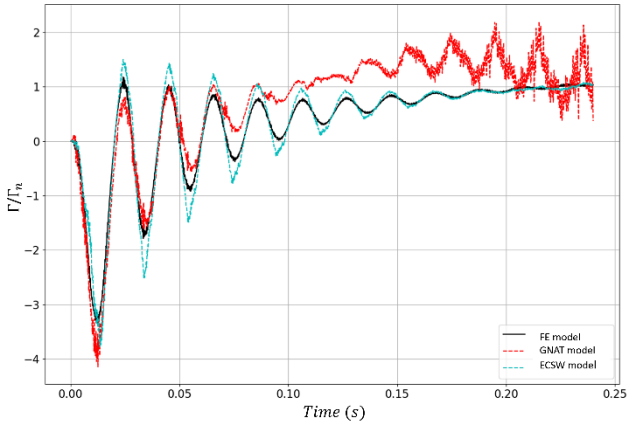

Figure 14. Electromagnetic torque from FE model (black), GNAT (red dashes) and ECSW (cyan dashes) at $U = 0.9U_n$

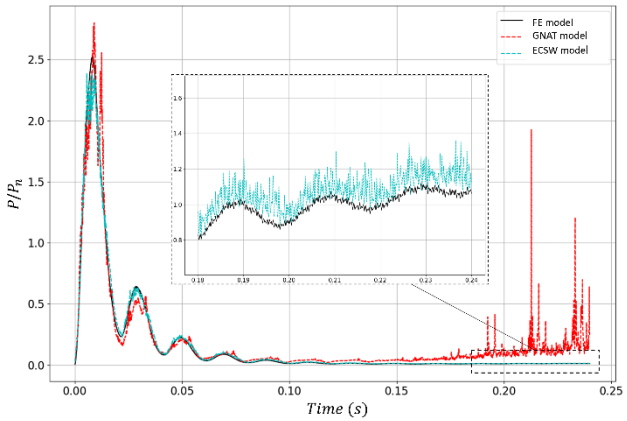

Figure 15. Eddy current losses from FE model (black), GNAT (red dashes) and ECSW (cyan dashes) at $U = 0.9U_n$

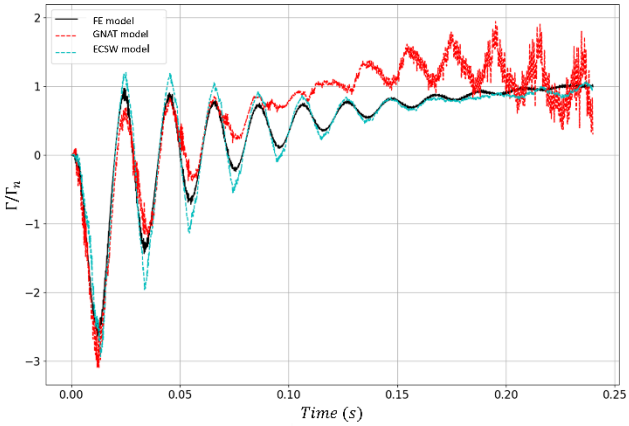

Figure 16. Electromagnetic torque from FE model (black), GNAT (red dashes) and ECSW (cyan dashes) at $U = 0.8U_n$

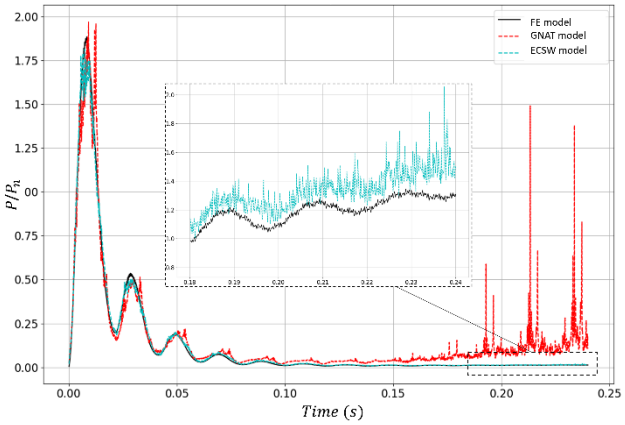

Figure 17. Eddy current losses from FE model (black), GNAT (red dashes) and ECSW (cyan dashes) at $U = 0.8U_n$

As in section V.D.2, we observe a similar deviation for both reduced models in transient regime, in all faulty regimes. Then, focusing on the electromagnetic torque (Figure 14 and Figure 16), the POD-ECSW reduced model yields a very good approximation of the evolution of this quantity in steady state, while the GNAT reduced model shows an important deviation and strong oscillations. When looking at the eddy current losses (Figure 15 and Figure 17), we can observe a huge difference in precision of the reduced models. The POD-ECSW model shows a deviation of a magnitude lower than 15%, while the GNAT model greatly overestimates this quantity in steady state. For practical application, an error of 15% is totally acceptable.

To sum up, we compute the average values of torque and losses in steady state regime and calculate the relative error to the FE reference. To do so, we first calculate the average value of the quantity of interest X over a chosen time interval (2 electrical periods in steady state) for FE model (X_{FE}), GNAT model (X_{GNAT}) and ECSW model (X_{ECSW}). Then, we determine the relative error of the reduced model average value compared to the FE average value, for GNAT as an example: $error_{GNAT} = \frac{|X_{GNAT} - X_{FE}|}{|X_{FE}|}$.

The values are shown on Table 1, as well as the online speedups of the reduced models compared to the FE model (to recall, simulations ran on a laptop with a i7-11850H @ 2.50GHz × 16 CPU).

Table 1. Relative error on electromagnetic torque and eddy current losses in steady state regime and online speedups.

	U_n ; ω_n	$0.9U_n$; $0.998\omega_n$	$0.8U_n$; $0.996\omega_n$
Electromagnetic torque relative error (%)			
GNAT	26,4	41,8	33,3
ECSW	2	3,8	8,3
Eddy current losses relative error (%)			
GNAT	59,5	2073,8	1493,4
ECSW	10,6	9,6	14,2
Speedups			
GNAT	40	30	37
ECSW	43	37	44

Looking at Table 1 confirms that the ECSW model yields a far better precision on both quantities of interest for all operating points when compared to the GNAT model. In terms of online speedup, both models show an important acceleration of the simulation, and allow to complete the simulation in a dozen of minutes when it takes 9h for the FE model. The POD-ECSW model gives better speedups which can be explained by a lesser number of elements on which the nonlinearities are approximated compared to the GNAT. These results suggest the possibility of using ECSW models in an industrial context, where a precision of 15% is more than acceptable with a speedup of about 40.

VI. Conclusion

The GNAT and ECSW methods combined with POD have been applied to construct a reduced model of a squirrel cage induction machine in nonlinear case. Based on the example shown here, it has been shown that the ECSW method enables to reduce the computation time by a factor 40 with an acceptable degradation of the quality of the results. Moreover, an approach based on the k-means algorithm has been proposed to reduce the memory resource and the computational time required to construct the reduced POD-ECSW model in the offline stage.

References

[1] L. Sirovich, Turbulence and the dynamics of coherent structures, Quarterly of Applied Mathematics, vol. 45, pp. 561-571, 1987.

[2] A. Ammar, B. Mokdad, F. Chinesta, and R. Keunings, A new family of solvers for some classes of multidimensional partial differential equations encountered in kinetic theory modeling of complex fluids, Journal of Non-Newtonian fluid Mechanics, vol. 139, no 3, p. 153-176, 2006.

[3] W. E. Arnoldi, The principle of minimized iterations in the solution of the matrix eigenvalue problem, Quarterly of Applied Mathematics, vol. 9, no 1, pp. 17-29, 1951.

[4] Y. Shindo, T. Miyazaki, and T. Matsuo, Cauer Circuit Representation of the Homogenized Eddy-Current Field Based on the Legendre Expansion for a Magnetic Sheet, IEEE Trans. on Magn., vol. 52, n° 3, pp. 1-4, 2015.

[5] M. Tobita and T, Matsuo, Nonlinear model order reduction of induction motors using parameterized Cauer ladder network Method, IEEE Trans. on Magn., vol. 58, pp. 8205504, 2022.

[6] D. Ryckelynck, A priori hyperreduction method: an adaptive approach, Journal of Computational Physics, vol. 202 n°1, pp 346–366, 2005.

[7] P. Astrid, S. Weiland, K. Willcox and T. Backx, Missing Point Estimation in Models Described by Proper Orthogonal Decomposition, IEEE Transactions on Automatic Control, vol. 53 n°10, pp. 2237– 2251, 2008.

[8] M. Barrault, Y. Maday, N. C. Nguyen and A. T. Patera, An 'empirical interpolation' method: application to efficient reduced-basis discretization of partial differential equations, Comptes Rendus Mathematique, vol. 339, n°9, pp. 667-672, 2004.

[9] R. Everson and L. Sirovich, Karhunen–loeve procedure for gappy data, JOSA A, vol. 12, n°8, pp. 1657-1664, 1995.

[10] K. Carlberg, C. Bou-Mosleh and C. Farhat, Efficient non-linear model reduction via a least-squares Petrov-Galerkin projection and compressive tensor approximations, International Journal for Numerical Methods in Engineering vol. 86, pp. 155-181, 2011.

[11] C. Farhat, P. Avery, T. Chapman et J. Cortial, Dimensional reduction of nonlinear finite element dynamic models with finite rotations and energy-based mesh sampling and weighting for computational efficiency, International Journal for Numerical Methods in Engineering, vol. 98, pp. 625-662, 2014.

[12] K. Carlberg, C. Farhat, J. Cortial and D. Amsallem, The GNAT method for nonlinear model reduction: effective implementation and application to computational fluid dynamics and turbulent flows, Journal of Computational Physics, vol. 242, pp. 623-647, 2013.

[13] M. R. Hasan, L. Montier, T. Henneron and R. Sabariego, Gappy-POD versus DEIM reduced-order model of a non-linear magnetodynamic problem, 12th International Conference on Scientific Computing in Electrical Engineering, pp. 95-96, EMF 2018.

[14] J. Maierhofer and D. J. Rixen, Model order reduction using hyperreduction methods (DEIM, ECSW) for magnetodynamic FEM problems, Finite Elements in Analysis and Design, vol. 209, 2022.

[15] Y. Kim, S.-H. Kang, H. Cho *et al,* Improved nonlinear analysis of a propeller blade based on hyper-reduction, *AIAA Journal*, vol. 60, no 3, pp. 1909-1922, 2022.

[16] I. A. Tsukerman, Overlapping finite elements for problems with movement, IEEE Trans. on Magn., vol. 28, pp. 2247-2249, 1982.

[17] L. Montier, A. Pierquin, T. Henneron, and S. Clénet, Structure preserving model reduction of low-frequency electromagnetic problem based on POD and DEIM, Trans. on Magn., vol. *53*, n° 6, pp. 1-4, 2017.

[18] M. Gu and S. C. Eisenstat, Efficient algorithms for computing a strong rank-revealing QR factorization. *SIAM Journal on Scientific Computing*, vol. *17*, n°4, pp. 848-869, 1996.

[19] R. Bro and S. De Jong, A Fast Non-Negative-Constrained Least Squares Algorithm, in Journal of Chemometrics, vol. 11, pp. 393-401, 1997.

[20] T. Delagnes, T. Henneron, S. Clénet, M. Fratila and J.-P. Ducreux, Comparison of reduced basis construction methods for Model Order Reduction, with application to non-linear low frequency electromagnetics. Mathematics and Computers in Simulation, vol. 211, pp. 470-488, 2023.

[21] T. Delagnes, T. Henneron, S. Clenet, and M. Fratila, Development of a FE Reduced Model on a Large Operating Range for a Squirrel Cage Induction Machine in Non Linear Case. In *2022 IEEE 20th Biennial Conference on Electromagnetic Field Computation (CEFC),* pp. 1-2, 2022.

[22] F. Piriou, A. Razek, "Finite element analysis in electromagnetic systems accounting for electrical circuit", IEEE Trans Mag, vol. 29, pp 1669-1675, 1993